The Effects of Film Structure and Surface Hydrogen on the Properties of Amorphous Carbon Films

G. T. Gao,[†] Paul T. Mikulski,[‡] Ginger M. Chateauneuf,[†] and Judith A. Harrison*[,†]

Department of Chemistry and Department of Physics, United States Naval Academy, Annapolis, Maryland 21402

Received: March 3, 2003; In Final Form: June 17, 2003

Molecular dynamics simulations were used to examine the mechanical and tribological properties of amorphous-carbon thin films with and without surface hydrogen. The simulations showed that the three-dimensional structure, not just the sp^3-to-sp^2 carbon ratio, is paramount in determining the mechanical properties of the films. Particular orientations of sp^2 ringlike structures create films with both high sp^2 content and large elastic constants. Films with graphite-like top layers parallel to the substrates have lower elastic constants than films with large amounts of sp^3-hybridized carbon. The layered structure of the hydrogen-free films caused them to have novel mechanical behavior, which also influenced the shape of the friction versus load data. The atomic-scale structure of the film at the interface was of critical importance in determining the load at which tribochemical reactions (or wear) between the counterface and films were induced.

1. Introduction

Diamond-like carbon (DLC) describes hydrogenated and hydrogen-free metastable amorphous carbon materials, prepared by a variety of chemical vapor deposition and plasma vapor deposition (PVD) techniques, that possess a wide range of mechanical and tribological properties.[1] Because of their potential as a solid lubricants, the growth mechanisms and the physical properties of amorphous carbon (*a*-C) films and diamond-like carbon (DLC) films have been the subject of intense experimental[1−6] and theoretical[7−14] interest. Solid lubricants may ultimately prove to be useful in a number of applications, including space-based technologies, computer hard disks, and microelectromechanical systems (MEMS).[15,16] Because of the large surface-to-volume ratios and low restoring forces, unwanted adhesion (stiction) and friction can dominate the performance of silicon-based MEMS.[17−19] A number of strategies have been proposed for the reduction of stiction and friction in MEMS including the use of amorphous carbon[20] or self-assembled monolayer[19,21] films as boundary-layer lubricants and the fabrication of MEMS from amorphous carbon and diamond.[22,23]

Amorphous carbon films can have a rich variety of structures depending upon the deposition process.[1,2,5,6] Experimentally, the ratio of 4-fold, diamond-like bonds to 3-fold, graphite-like bonds (sp^3-to-sp^2 ratio) and hydrogen content determine the kind of structures obtained. These DLC films exhibit a wide range of sometimes contradictory tribological properties. For instance, the friction of most DLC films increases with time when tested in inert environments. However, some films exhibit superlow friction when tested under similar conditions.[1,24,25] With these things in mind, it is clear that a fundamental understanding of the friction and wear mechanisms of DLC at the atomic scale is needed to design films with the desired tribological properties.

Previously, we investigated the atomic-scale friction and wear in two systems composed of hydrogen-terminated diamond (111) surfaces in sliding contact with *a*-C films using molecular dynamics (MD). Two *a*-C films with approximately the same surface and bulk structures and sp^3-to-sp^2 ratio of carbon atoms but with different thicknesses were examined.[26] Because of the similar structure at the interface, similar tribological behavior was found in the two films. Above a critical load, a series of tribochemical reactions occurred in both systems between the counterface and the film, which resulted in significant restructuring of the films. This restructuring caused a lowering of friction consistent with "run-in" behavior observed in macroscopic DLC friction experiments.[1] Because the three-dimensional atomic-scale structure of both films was similar, the effects of film structure on mechanical and tribological properties were not studied. This work is aimed at shedding light on the influence of film structure (both surface and bulk) on tribological and mechanical properties using MD simulations. Specifically, it will discuss how strain and friction change with load in five films with different three-dimensional bond-network structures. Sliding-induced restructuring and tribochemical reactions were also investigated. Of the five films discussed in this paper, three films are hydrogen-free (*a*-C) and two films contain surface hydrogen (*a*-C:H).

2. Method

The simulation systems consist of diamond (111) counterfaces that are brought into sliding contact with *a*-C films attached to the (111) surface of diamond. In all cases, the diamond substrate and the diamond counterface contain seven layers of carbon atoms with 144 atoms per layer. The diamond counterface is terminated with hydrogen atoms to satisfy the valence requirements of carbon. Periodic boundary conditions are applied in the plane defined by the film, and the dimensions of the computation cell in the plane containing the film are 30.2 Å by 26.1 Å (12 diamond (111) unit cells in the sliding direction and 6 diamond (111) unit cells perpendicular to the sliding direction).

The forces acting on each atom are derived from Brenner's reactive empirical bond-order (REBO) potential.[27−30] The many-

* To whom correspondence should be addressed. E-mail: jah@usna.edu.
[†] Department of Chemistry.
[‡] Department of Physics.

10.1021/jp034544+
Published on Web 09/13/2003

body nature of the REBO potential allows the bond energy of each atom to depend on its local environment. Thus, chemical reactions that may accompany compression or sliding are possible in this model. The REBO potential contains a term to account for the torsional force across carbon−carbon double or triple bonds.[28] It has been shown that this form of the REBO potential accurately represents the energies, bond lengths, and lattice constants of solid- and gas-phase hydrocarbon materials.

Recent MD simulations utilized this potential to examine the liquid−liquid phase transformation in carbon.[12] The potential produced sp^3-dominated diamond-like structures at high densities and chainlike structures (sp-dominated) at low densities. Furthermore, the presence of the torsional term in the REBO potential was shown to be critical for formation of sp^3-dominated structures.[12] With this term "turned off", a quenched liquid-carbon system contained almost all sp^2-hybridized carbon atoms, even at densities as high as diamond. From this work, it can be inferred that the structure of a film can be altered by changing its density or scaling the torsional term of the REBO potential between 0 and 1 in the simulations of the melting and quenching processes.[12] This latter method was utilized to generate the films discussed in this work.

An updated version of the REBO potential was introduced recently. This version more accurately reproduces the elastic constants of diamond and graphite while not disrupting the properties that were fit in the original version of the potential.[29,30] Unless otherwise noted, the compression and sliding simulations reported here were conducted using this updated REBO potential.

In all of the simulations reported here, the bottom two layers of the diamond substrate and the top two layers of the counterface are held rigid. Because the outermost layers are held rigid, their relative position defines the interface separation, and thus, the applied load. Moving inward toward the carbon film, the next three layers of the substrate and the counterface are maintained at a constant temperature (300 K) using a Berendsen thermostat.[31] All remaining atoms are free to move according to Newton's equations without additional constraints. The equations of motion for all nonrigid atoms are integrated using the fifth-order Gear predictor−corrector algorithm with a constant step size of 0.25 fs.[32] The load and friction are taken to be the forces on the rigid layer atoms that are parallel to the compression and sliding directions, respectively.

Our previous molecular dynamics study also examined friction in amorphous carbon films.[26] In that work, two films with different thicknesses but identical surface structures had similar average friction in the load range examined. This suggests that the structure of the film at the interface plays an intimate role in governing friction. With that in mind, careful attention was paid to quantifying the structure of the films examined in this work. The local coordination between a given pair of atoms is one way to represent the structure of a film. However, as the atoms within a film vibrate around their equilibrium positions, the distance between each pair of atoms is also in oscillation. Thus, the local coordination of each atom may also oscillate during the simulation. Our analysis of the bond-length vibrations within the film during the course of several simulations reveals that two atoms are bound when their minimum distance is always below R_{min} and their maximum distance never exceeds R_{max}. The values of R_{min} for carbon−carbon, carbon−hydrogen, and hydrogen−hydrogen pairs are 1.7, 1.3, and 1.1 Å, respectively. The values of R_{max} for the same pairs are 1.94, 1.75, and 1.64 Å, respectively.[33]

Amorphous carbon films are made by vapor deposition techniques, where the technique and the deposition process control the structure of the film. It is also possible to simulate the deposition.[9,34,35] However, this is not the most computationally efficient way to generate *a*-C films with differing surface structures. Two other widely used simulation methods for generating *a*-C films are homogeneous condensation of a vapor and ultrafast quenching of liquid carbon.[7,10−13,36] The *a*-C films used in our previous work were created by melting a piece of diamond then rapidly cooling it to room temperature while contact was maintained with the substrate.[26] Although this method is simple and effective, it is difficult to generate *a*-C films with different structures. A similar approach, which also suffers from the same lack of structure control, was used by Sinnott et al.[37]

The *a*-C films examined here are created by cooling liquid carbon that is confined between two diamond (111) surfaces. Hydrogen and carbon atoms are confined between diamond surfaces to create the hydrogen-containing films. One diamond surface, which becomes the substrate, is not terminated with hydrogen atoms. Hydrogen atoms are added to all of the unsaturated carbon atoms on the second diamond surface. Starting from random configurations, the confined film atoms are heated to 6000 K (T_0), while the two diamond surfaces are held rigid. For the hydrogen-containing films, the hydrogen atoms are randomly placed throughout the starting film. After the films are equilibrated at T_0, they are quenched to room temperature using an exponential cooling curve of the form $T = T_0\, e^{-ct}$, where T, t, and c are temperature, time, and a constant, respectively. The quenching times are on the order of 100 ps. It should noted that these rather long quench times allowed the bulk of the hydrogen atoms to migrate to the surface of the films. Shorter quench times "trap" the hydrogen atoms within the films. After the film is quenched, the films form multiple bonds with the substrate and no bonds with the saturated diamond surfaces. Last, the diamond surface that is not bonded with the film is removed and the remaining atoms are allowed to equilibrate.

3. Results

3.1. Structure. Five amorphous films were generated and their final structures and various quantities associated with each film are shown in Figure 1 and Table 1, respectively. Films IV and V contain hydrogen atoms, which are mostly confined to the surfaces of the films, while films I−III are hydrogen-free. The percentages of sp^3-hybridized carbon atoms and the corresponding calculated densities are comparable to what can be obtained experimentally.[1,2,38]

Average density profiles were calculated after the films were equilibrated at 300 K. The density information from 250 configurations, separated by 10 ps, was used to calculate the average density profiles for all films. Density profiles for uncompressed films I and IV are shown in in Figure 2. The uncompressed density profiles for films II and III are similar to that of film I and the profile for film V is similar to that of film IV. In general, all of the films form layered structures. Each atom in the bottom layer of the films forms a bond with the diamond substrate, which corresponds to the peak in the density profiles at approximately 1.5 Å (the diamond substrate is located at 0.0 Å). Above this layer, the bonding network in each film varies and the films become less structured. Films I, IV, and V are composed predominantly of sp^3-hybridized carbon, which is also apparent from the bond-angle and bond-direction distributions ($g(\theta)$) within the films (Figure 3). In addition, the

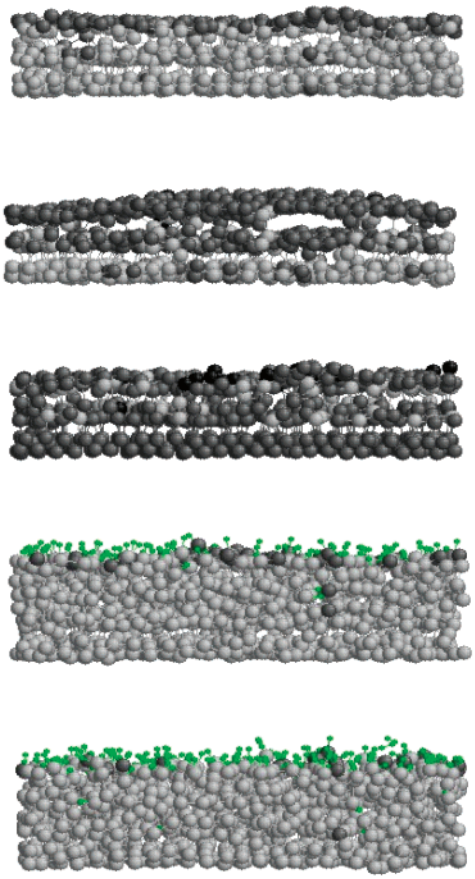

Figure 1. Snapshots of the amorphous films examined in this work. Beginning from the top and going down the page are films I−V. Large gray and black spheres represent sp^3-hybridized and sp^2-hybridized carbon atoms, respectively. Small green spheres represent hydrogen atoms. The films are attached to diamond (111) substrates (below the films), which are not shown. The hydrogen-terminated diamond (111) counterface (above the films) is also not shown.

TABLE 1: Film Composition and Properties

film	C	H	sp^3 (%)	sp^2 (%)	sp (%)	h_0 (Å)	d (g/cm^3)	avg coord	c_{zz} (GPa) (% error)
I	837	0	73.6	26.4	0.0	7.10	2.98	3.71	144 ± 9.8
II	837	0	38.7	60.7	0.60	7.70	2.75	3.33	117 ± 11
III	837	0	14.9	82.4	2.6	7.65	2.77	3.09	267 ± 4.4
IV	1115	120	94.4	5.6	0.0	9.95	2.86	3.92	462 ± 4.2
V	1075	200	97.5	2.5	0.0	10.38	2.66	3.97	449 ± 6.7

majority of interlayer bonds are between tetrahedrally bonded carbon atoms. The majority of the sp^2-hybridized carbon atoms in these films are found near the surface (close to the counterface). In film I, the sp^2-hybridized carbon atoms form ringlike structures that lie in the plane *parallel* to the substrate. This arrangement of ringlike structures reduces the amount of interlayer bonding between the top two layers.

Both films II and III have a larger percentage of sp^2-hybridized carbon than sp^3-hybridized carbon atoms. However, the three-dimensional arrangement of the rings of sp^2-hybridized atoms differs in each film. In film II, the top two layers contain the bulk of the sp^2-hybridized carbon atoms and they form ringlike structures that lie in the plane *parallel* to the substrate (similar to film I). In contrast, the bulk of the ringlike sp^2-hybridized structures are *perpendicular* to the diamond substrate in film III. Close to the diamond substrate, adjacent layers in film III are predominantly connected by bonds between these sp^2-hybridized carbon atoms. Farther from the substrate, the interlayer bonds are composed of both sp^2- and sp^3-hybridized carbon atoms.

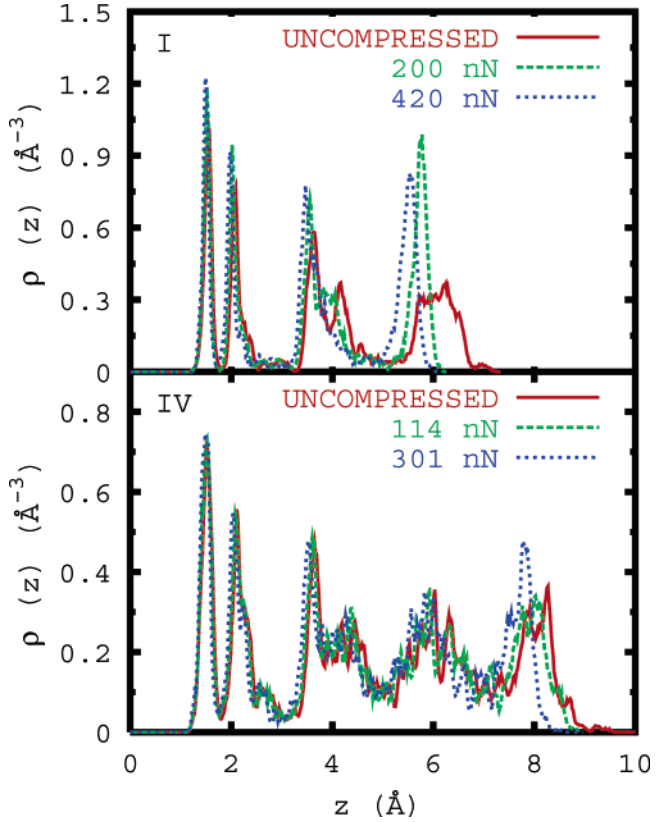

Figure 2. Density profiles at 300 K for the uncompressed and compressed films. Films I (0, 200, and 420 nN) and IV (0, 114, and 301 nN) are in the upper and lower panels, respectively. Calculation details are given in the text.

Insight into the bonding structure within the films is also apparent from an examination of the angle (θ) between the plane containing the diamond substrate and a given chemical bond within a film. The distribution of these angles is shown for all films in Figure 3. With the use of this definition of θ, peaks near 0° and 90° correspond to chemical bonds that are parallel and perpendicular to the diamond substrate, respectively. Thus, films that have ringlike structures parallel to the substrate have peaks near 0° (films I and II). Film III has a peak near 90° because of its interlayer sp^2-hybridized carbon atoms. Films I, II, IV, and V have a significant fraction of sp^3-hybridized carbon atoms and thus have a peaks near 20°, while the mostly sp^2-hybridized film III has a large peak near 30°.

3.2. Compression. Compression of the amorphous films was accomplished by moving the rigid layers of the diamond (111) countersurface at a constant velocity of 10 m/s toward the films. Because periodic boundary conditions were applied in the plane that contains the films, deformation of the films during compression was measured by changes in their relative thicknesses. The change in thickness, or strain, is defined as $\epsilon_{zz} = |\Delta h/h_0|$, where h_0 is the thickness of an uncompressed film and Δh is the change in thickness upon compression. Figure 4 shows the load as a function of ϵ_{zz} for the five films.

It is clear from an analysis of Figure 4 that there is not one distinct value of the slope for each film. This is likely because the films are layered. As the strain is increased, it is also possible the underlying substrate begins to have an influence. For very small values of strain (less than 0.02), the data in Figure 4 are approximately linear and the slope of each line is related to the elastic constant of the film in the compression direction. For

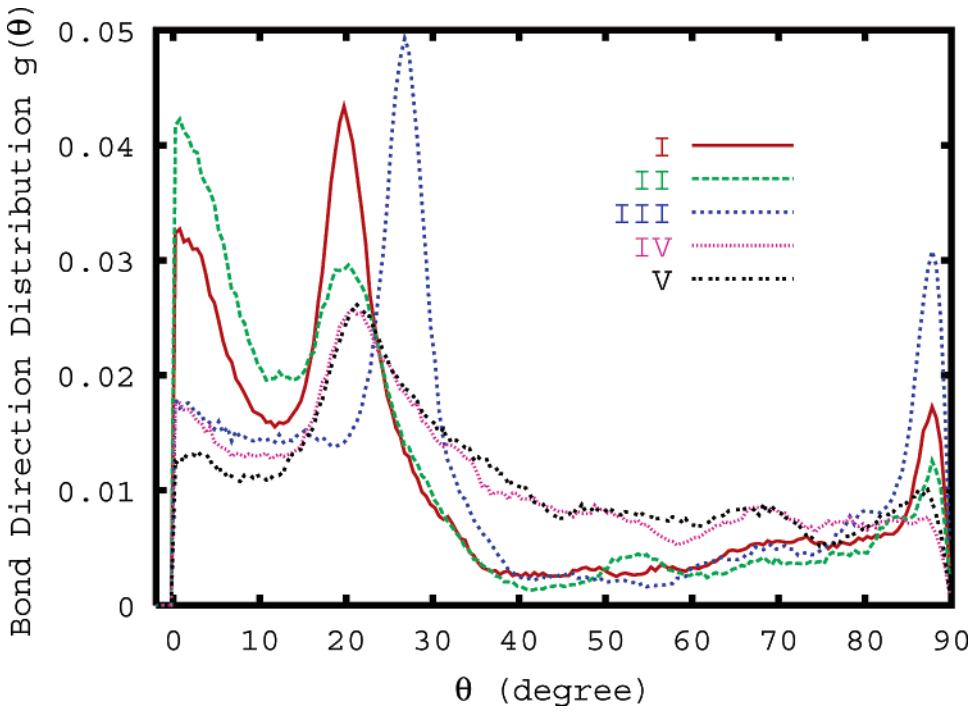

Figure 3. Bond-direction distribution $g(\theta)$ as a function of angle θ. The angle θ is defined as the angle between the plane that contains the diamond substrate and a given chemical bond within the film.

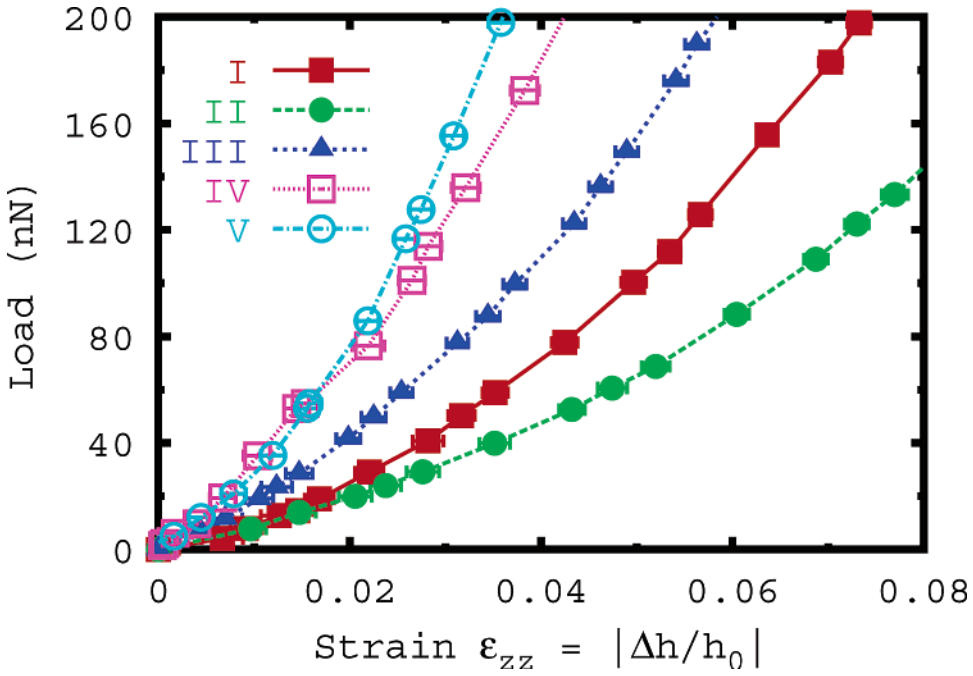

Figure 4. Load on the rigid layers of the diamond probe as a function of strain, ϵ_{zz}, of the films.

convenience, we will refer to this constant as c_{zz}. In this region, linear fits were obtained, and the c_{zz} values are shown in Table 1. These values are on the lower end of the range of Young's modulus values determined experimentally[39,40] and a bit lower than calculated values of c_{11}.[41] Ferrai et al. used Brillouin scattering to determine the Young's and shear moduli of isotropic and layered tetrahedral amorphous carbon films.[42] Scattering results showed that layered films typically have lower moduli values than isotropic films.

In general, increasing the average coordination, or the sp^3-to-sp^2 ratio of carbon in the films, increases the elastic constant in the compression direction. This trend has been reported in experiments[42] and previous calculations.[41] However, despite the fact that film III is dominated sp^2-hybridized carbon atoms and has the lowest average coordination, its elastic constant is larger than that of film I or II. This arises from the three-dimensional arrangement of atoms within the film. Because the majority of the sp^2-hybridized ringlike structures are perpendicular to the substrate, there are more interlayer bonds in film III than there are in the other hydrogen-free films, making it more difficult to compress.

In film II, the majority of carbon atoms in the top two layers (Figure 1) form sp^2-hybridized ringlike structures that are parallel to the plane containing the substrate. This three-dimensional arrangement of ringlike structures gives rise to fewer interlayer bonds between the first two layers of the film

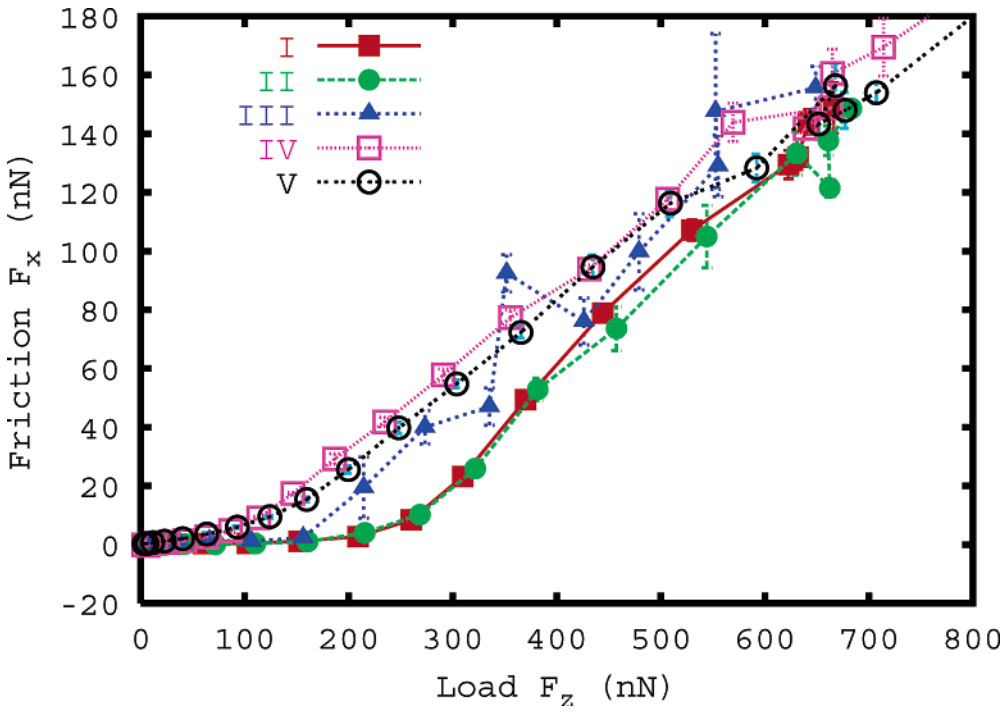

Figure 5. Average friction as a function of average load for the five films shown in Figure 1. Lines have been drawn to aid the eye.

compared to the other hydrogen-free films. Thus, film II undergoes a greater degree of deformation for a given applied load and appears less stiff than any of the hydrogen-free films. For small strains, the load versus strain data for film I are approximately the same as those for film II. This is likely due to the similar structure of the two films near the interface.

Because the hydrogen-containing films are largely composed of sp^3-hybridized carbon atoms, they undergo smaller strains at a given load than the hydrogen-free films and have larger elastic constants. Further differences in the hydrogen-free versus hydrogen-containing films are apparent upon examination of the density profiles of films I and IV at various loads (Figure 2). The application of load results in a significant thinning of top layer of film I. This is manifest as a change in width of the peak at large values of z in Figure 2. In addition, the spacing between layers is also decreased upon compression. This change in interlayer spacing is small compared to the change in thickness of the topmost layer. The density profiles of film II as a function of load look much the same as those of film I. In contrast, because the hydrogen-containing films contain a uniform sp^3-hybridized network of atoms, there is little change in top-layer thickness or interlayer spacing upon compression (Figure 2). Thus, the mechanical properties of these layered films are intimately linked to the underlying three-dimensional arrangement of atoms within the films. The average coordination, or sp^3-to-sp^2 ratio of carbon atoms, alone is not enough to predict mechanical properties of the films.

3.3. Friction. To investigate the relationship between film structure and tribological properties, sliding simulations were performed. Sliding of the counterface was accomplished by moving the rigid layers of the counterface at a constant velocity (100 m/s) in the sliding direction while maintaining a constant separation between the rigid layers. To determine the friction−load relationship, sliding simulations were performed at several fixed separations (loads) in each system. At each load, the initial configuration for sliding was extracted from the compression simulation.

Figure 5 shows the average friction as a function of the average load for the five film systems examined here. To eliminate the influence of startup effects that arise from the abrupt transition from compression to sliding, data from the first 15 ps of sliding are ignored in all of the sliding simulations. Data from the next 15 ps of sliding are partitioned into six unit-cell bins. The instantaneous friction (load) in each cell is averaged, and these unit-cell averages are used to obtain the friction (load) values reported in Figure 5. The error bars represent one standard deviation of the average friction from the six unit-cell bins for a given slide.

Friction curves for films I and II are nearly identical over the entire load range. The curves for films IV and V are also statistically equivalent. In general, these two sets of friction curves are composed of three regions. In films I and II, the friction is quite low, appearing "flat" from loads of 0 to approximately 200 nN. Between approximately 200 and 600 nN, the friction curves are linear. Beyond 600 nN, the curves become irregular because of tribochemical reactions between the counterface and the film. These reactions will be discussed in the next section. In the lowest load regime, the application of load results largely in compression of the topmost layer of the film (Figure 2). Because it is easy to compress sp^2-hybridized rings in this orientation, the friction changes little in this region. Between 200 and 400 nN, the thickness of the topmost layer changes little and the compression of the entire film is more uniform (Figure 2). Thus, the friction increases markedly after 200 nN. Because the friction versus load data are not linear over the entire load range examined, computation of a friction coefficient is problematic. However, it is possible to extract a *local* friction coefficient in the intermediate load range where these data are linear. These so-called *local* friction coefficients for films I and II are statistically equivalent and on the order of 0.325 ± 0.014.

In films IV and V, the friction is quite low between 0 and approximately 100 nN. In the intermediate load regime (approximately 100 to 600 nN), these curves are linear and after approximately 600 nN tribochemical reactions between the

counterface and film occur. When compared to the hydrogen-free films in the low-load region, the friction for these films is not as "flat" and the transition to region two begins at lower values of load. The compression of the layers is more uniform as the load is applied because the films are composed of a three-dimensional network of sp^3-hybridized carbon atoms that is more uniform than those of the other three films. In the intermediate load regime, the *local* friction coefficients for films IV and V are *lower* than those for films I and II with a value of 0.268 ± 0.008 (these coefficients are statistically equivalent for films IV and V). However, the average friction of films IV and V is consistently *larger* than the friction of films I and II at a given load. The relative position of the friction curves of films I and II at a given load compared to films IV and V arises from the differences in their response to compression. Finally, while there is not a statistically significant difference in the friction of films IV and V over the load range examined, it is interesting to note that the average friction of film IV is consistently larger than the friction of film V.

Previous MD simulations examined friction of a nonlayered film composed mostly of sp^2-hybridized carbon atoms using the same counterface used here.[26] Because this film was not layered, the friction versus load data did not possess the "flat" region at low load exhibited by the films discussed here.

While the *local* friction coefficients obtained here are in the range of those obtained experimentally,[1,2] exact comparison of these numbers is problematic due to differences in experimental and simulation conditions. These *local* friction coefficients are reflective of the interactions present between the counterface and the films during sliding. Previous MD simulations and early models of wearless friction[43,44] show that increasing the extrema of the potential between the sliding surfaces leads to an increase in friction.[45] One of these early models makes the connection between the potential extrema and friction in the following way. Two atomically flat solids, A and B, are in sliding contact. The B solid has surface atoms (B_0) attached to it by harmonic springs, which lose energy to the surface via vibration. As the surfaces slide over one another, any given B_0 atom experiences the potential, V_{AB}, arising from the interaction of the two surfaces. It is the shape of V_{AB} that ultimately governs the friction process. For strongly interacting surfaces, V_{AB} will contain various local extrema. A given B_0 atom passes though various metastable local minima upon sliding. Falling from these metastable minima to a lower minimum causes B_0 to become vibrationally excited, a process termed "plucking". This vibrational energy is then dissipated to the solid as heat. Thus, plucking results in strain energy of translation being converted to vibrational energy, which is the essence of the atomic-scale friction process. For very weakly interacting solids, the friction vanishes because V_{AB} would contain no metastable local minima.

In films I and II, the interactions across the interface are nonbonded C···H interactions. In contrast, in films IV and V, the majority of the interactions are nonbonded H···H interactions between the films and the counterface. In an effort to examine the interfacial potential extrema, a hydrogen molecule in an orientation perpendicular to the films was scanned over the surfaces of films I and IV and the potential energy calculated. The potential energy contour diagrams generated using this procedure show that the potential between and hydrogen molecule and film IV (H···H) is weaker than that between film I and a hydrogen molecule (C···H) in the same orientation at the same distance from the film. Thus, there is less energy dissipation when the counterface is in sliding contact with films IV and V and lower friction.

The friction curve for film III is composed of only two regions. At loads below approximately 150 nN, the friction of film III is indistinguishable from films I and II and is quite small. Above this load, the curves become irregular due to tribochemical reactions between the counterface and the film. Again, the initial application of load results largely in a change in thickness of the topmost layer and a slight change in interlayer spacing. Because film III has more interlayer bonds than any of the hydrogen-free films, this flat region does not persist to as high loads as it does in films I and II.

3.4. Tribochemistry. Experiments have shown that chemical reactions induced by sliding significantly impact the friction of DLC.[1,4,5,46−48] Molecular dynamics simulations have also been used to examine the tribology of *a*-C films.[26] These simulations revealed that sliding of the counterface can alter the structure of the *a*-C film by inducing a series of bond-breaking and bond-forming events. These events occurred within the film (intrafilm) at all loads and between the counterface and the film (interfilm) after a critical load was reached. If a significant number of interfilm bonds formed, the friction increased dramatically because of the adhesion between the counterface and the film. In some cases, tribochemical reactions significantly altered the structure of the film leading to lower friction.

Both intrafilm and interfilm reactions are found in the systems examined here. However, the critical load required for initiation of interfilm reactions differs depending upon the structure of the films. Loads of 450 and 620 nN are required to initiate interfilm reactions in films II and I, respectively. In contrast, despite the fact that film III has the largest elastic constant among the hydrogen-free films, its surface structure causes interfilm reactions to be initiated at much lower loads (150 nN). A series of typical interfilm reactions in film III is shown in Figure 6. The surface of film III contains a number of unsaturated sp-hybridized carbon atoms. These atoms serve as initiation points for chemical reactions between the counterface and the film. Formation of these bonds leads to the transfer of counterface atoms to the film and significant restructuring of the film. It is the formation of adhesive bonds between the counterface and the film that cause the irregular nature of the friction versus load data (Figure 5) and the friction of film III to be larger than the other hydrogen-free films at most loads.

The number of bonds formed and broken in film II during sliding is shown in Figure 7 for two loads. The lower panel of Figure 7 shows that there is a fairly small number of intra- and interfilm reactions in film II at low loads. Both intra- and interfilm reactions increase slowly with sliding distance, and the number of reactions is constant after approximately 80 Å of sliding. Increasing the load causes a marked increase in the number of tribochemical reactions (Figure 7, middle panel). The number of reactions increases monotonically with sliding distance during the first 70 Å of sliding. At this point, the bond network stabilizes and the number of reactions is fairly constant. Thus, the film has achieved a near steady-state structure, one with a slightly lower average friction than that present at the start of the sliding (Figure 7, upper panel). That is, the oscillations in friction with distance are smaller, and the average friction is lower. A more dramatic example of this atomic-scale behavior was observed in our previous simulations[26] and may be analogous to "run-in" observed in friction experiments on nanocrystalline diamond.[25] Because the number of tribochemical reactions in *a*−C films is a function of distance, it is important to keep the simulation distances constant when calculating and reporting friction.

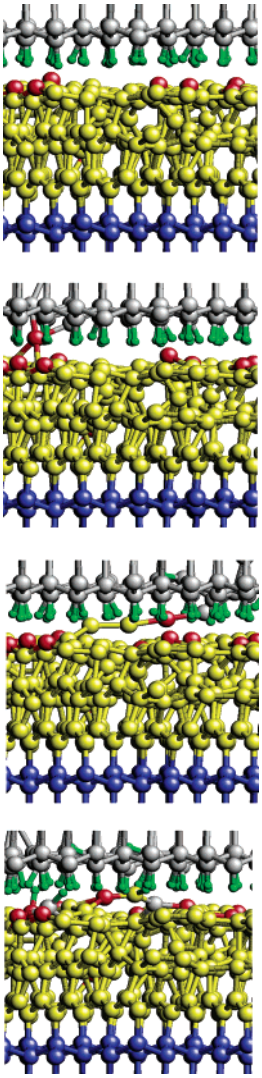

Figure 6. A series of chemical reactions induced when the counterface is in sliding contact with film III under a load of 230 nN. Beginning from the top of the page, the counterface has slid 0.0, 13.5, 23.5, and 144.5 Å in each panel. Prior to sliding (top panel), several unsaturated sp-hybridized carbon atoms (red) are present on the surface of the film. A chemical bond is formed between the diamond counterface (gray) and the sp-hybridized atom (second panel from top). Both the counterface and the film undergo significant restructuring as a result of the adhesive bond formation (second panel from bottom). In this panel, a number of atoms are being "pulled" from the film. Continued sliding causes adhesive bonds to rupture leading to the transfer of counterface atoms to the film and significant restructuring of the film (bottom panel). Counterface carbon and hydrogen atoms are shown in gray and green, respectively. Unsaturated sp-hybridized atoms in the film are shown in red and the remaining film atoms are shown in yellow. Diamond substrate atoms are shown in blue.

Analysis of the changes in hybridization of film II during sliding reveals a more detailed analysis of the intrafilm reactions. While the total number of sp^2-hybridized and sp^3-hybridized carbon atoms is approximately constant, the relative number of each changes (Figure 8) during sliding. There is a marked drop in the number of sp^2-hybridized carbon atoms and a concomitant increase in the number of sp^3-hybridized carbon atoms during the first 30 ps of sliding. Continued sliding causes a slight reduction (increase) in the number of sp^3-hybridized (sp^2-hybridized) atoms. In the last 40 ps of sliding, the number of both types of atoms is fairly constant.

Interfilm reactions are initiated at approximately 710 and 840 nN in films IV and V, respectively. Thus, for the films examined here the general trend is an increase in the critical load required for interfilm reaction initiation with increasing amount of sp^3-hybridized carbon atoms. The surfaces of the hydrogen-free films (except film III) are dominated by sp^2-hybridized carbon atoms in the plane that is parallel to the substrate.

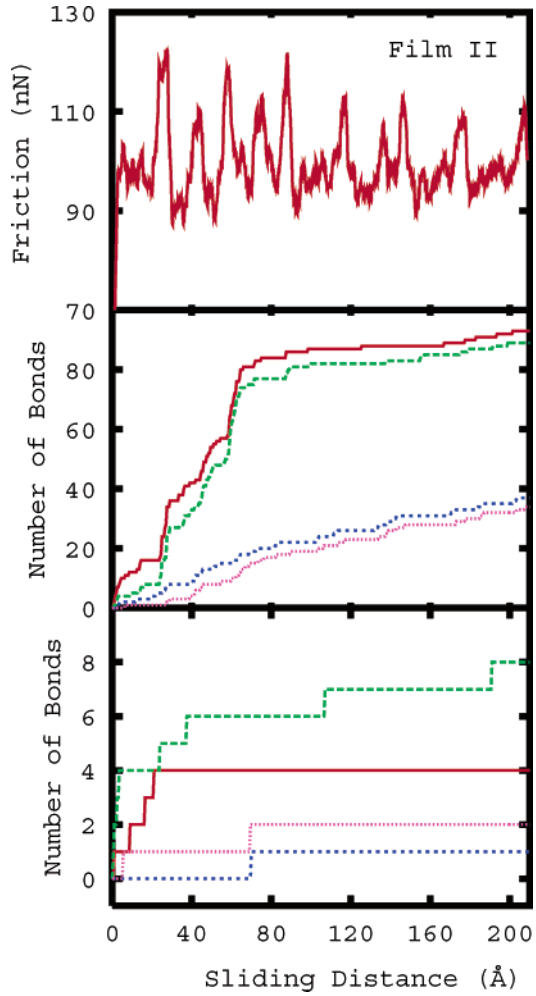

Figure 7. The number of inter- and intrafilm bonds formed and broken during a given sliding simulation. Data for film II at a load of 320 nN and at a load of 545 nN are shown in the lower and middle panels, respectively. The red (solid) and green (dashed) lines represent intrafilm bonds formed and broken, respectively. The blue (dot−dashed) and pink (dotted) lines represent interfilm bonds formed and broken, respectively. Instantaneous friction as a function of sliding distance at 545 nN is shown in the upper panel.

There are several loads at which the friction of film III is larger than that of either of the hydrogen-containing films because of the large number of interfilm reactions that occur between the film and the counterface. In contrast, both hydrogen-containing films undergo few interfilm reactions even at large loads. After the counterface has slid for 200 Å on film V under an average load of approximately 590 nN, very few interfilm bonds have been formed (two) or broken (one) and a small number of intrafilm reactions occur (15−20). During the sliding, the sp^3-hybridized bonds are broken and converted to sp^2-hybridized bonds within the films. Thus, the number of bonds broken within these films is larger than the number of bonds formed. This is true at all loads for both hydrogen-containing films.

4. Summary

The three-dimensional arrangement of atoms within the film is of critical importance when determining the mechanical and

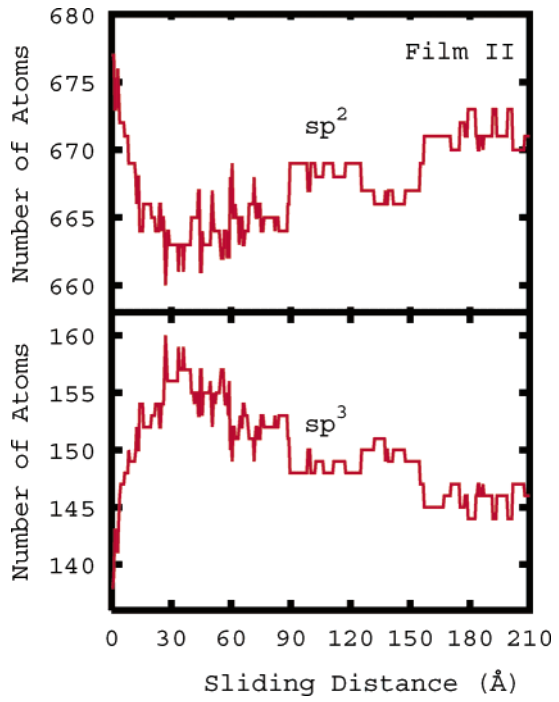

Figure 8. The number of sp^2- (upper panel) and sp^3-hybridized (lower panel) carbon atoms as a function of sliding distance for film II at 545 nN.

tribological properties of a film. That is, the sp^3-to-sp^2 hybridization ratio alone does not always provide enough information to predict the mechanical or tribological behavior of a film. For example, the formation of sp^2-hybridized rings that are oriented perpendicular to the substrate leads to films with larger elastic constants than would be predicted by using the ratio of sp^3-to-sp^2 carbon.[2,39] In the absence of this type of structural feature, the elastic constants of the films examined here follow the conventional trend of increasing with increasing sp^3 carbon content. Because the films were layered, initial application of load caused an uneven strain with the topmost layer being compressed the largest amount. This layering lead to elastic constants in the compression direction that were smaller than would be predicted using sp^3-to-sp^2 hybridization ratio alone. Lower values of Young's modulus and hardness have been measured experimentally for layered films.[42]

The structure of the film near the interface is the critical factor in determining friction. Our previous simulations have shown that nonlayered films with nearly identical surface structures, but different thicknesses, have similar friction.[26] In this work, films with similar surface structures, films I and II and films IV and V, manifest similar average friction through the entire load range examined. When the interface is dominated by nonbonded H···H interactions, the *local* friction coefficients (evaluated in the linear region of the friction versus load data) are lower than when C···H nonbonded interactions dominate. Chemical reactions between the probe and the counterface increase friction and are responsible for the erratic, nonlinear appearance of the friction curves. These reactions occur at lower loads when unsaturated sp atoms are present near the surface of the film.

While the surface structure is critical in determining friction, it should also be noted that the surface structure is intimately linked to the structure of the bulk film. In nonconductive systems, energy is dissipated via excitation of phonons. Because the three-dimensional structure of the hydrogen-containing films is very different from that of the hydrogen-free films, the phonon frequencies are likely to be different. Thus, it is difficult to quantify how much of the calculated differences in friction arise from phonon frequency differences and how much from the change in surface structure. In the hydrogen-containing films, the bulk structure of the films is similar. As a result, it is likely that the phonon modes in these two films are similar and that any small differences in average friction arise from the subtle changes in surface structures due to different amounts of hydrogen. The quantitative link between film structure and phonon frequencies is currently under investigation.

It has been shown that the friction of DLC films is strongly affected by the presence of hydrogen, hydrogen contents over 40% leading to a decrease in friction in ultrahigh vacuum (UHV).[1,2,6,49] Hydrogen atoms can be bound to carbon atoms throughout the film (sp^3-hybridized carbon can have one or more hydrogen atoms bound to it[50]) and can be present interstitially.[51] In the hydrogen-containing films examined here, the bulk of the hydrogen atoms migrated to the surface of the films during quenching. Thus, the hydrogen atoms in these simulations largely serve to passivate the surfaces leading to H···H interactions at the interface. As a result, these films are not representative of the DLC films that are generated experimentally. However, these simulations do provide insight into the way surface hydrogen can affect the surface of DLC films and thus influence friction. The effect of bound hydrogen atoms present throughout the films, or atoms present interstitially, on friction is the subject of current simulations.

Tribochemical reactions between the counterface and the film can contribute markedly to the calculated friction by increasing the adhesive component of friction. Unsaturated sp atoms on the surfaces of a film serve as initiation points for these reactions. Interfilm reactions are initiated at lower loads when these atoms are present on the surface. The two hardest films, which were dominated by sp^3-hybridized carbon and passivated with hydrogen, were the most resistant to interfilm reactions, or wear.

Acknowledgment. This work was supported by The Air Force Office of Scientific Research (AFOSR) and The Office of Naval Research (ONR) under Contracts NMIPR035203542 and N00014-03-WX-2-0412, respectively. J.A.H. also thanks R. W. Carpick, K. J. Wahl, A. Erdemir, and I. L. Singer for many helpful discussions.

References and Notes

(1) Erdemir, A.; Donnet, C. Tribology of Diamond, Diamond-Like Carbon, and Related Films. In *Modern Tribology Handbook*; Bhushan, B., Ed.; CRC Press LLC: Boca Raton, FL, 2001; pp 871−908 and references therein.
(2) Robertson, J. *Mater. Sci. Eng., R* **2002**, *37*, 129−281 and references therein.
(3) Fontaine, J.; Donnet, C.; Grill, A.; LeMogne, T. *Surf. Coat. Technol.* **2001**, *146−147*, 286−291.
(4) Huu, T. L.; Schmitt, M.; Paulmier, D. *Surf. Sci.* **1999**, *433−435*, 690−695.
(5) Grill, A. *Surf. Coat. Technol.* **1997**, *94−95*, 507−513.
(6) Robertson, J. *Surf. Coat. Technol.* **1992**, *50*, 185−203.
(7) Marks, N. A.; Cooper, N. C.; McKenzie, D. R. *Phys Rev. B* **2002**, *65*, 075411-1−075411-9.
(8) Kelires, P. C. *Diamond Relat. Mater.* **2001**, *10*, 139−144.
(9) Jager, H.; Albe, K. *J. Appl. Phys.* **2000**, *88*, 1129−1135.
(10) Bilek, M. M. M.; McKenzie, D. R.; McCulloch, D. G.; Goringe, C. M. *Phys. Rev. B* **2000**, *62*, 3071−3077.
(11) McCulloch, D. G.; McKenzie, D. R.; Goringe, C. M. *Phys. Rev. B* **2000**, *61*, 2349−2355.
(12) Glosli, J. N.; Ree, F. H. *Phys. Rev. Lett.* **1999**, *82*, 4659−4662.
(13) Marks, N. A.; McKenzie, D. R.; Pailthorpe, B. A.; Bernasconi, M.; Parrinello, M. *Phys. Rev. Lett.* **1996**, *76*, 768−771.
(14) Stephan, U.; Haase, M. *J. Phys.: Condens. Matter* **1993**, *5*, 9157−9168.

(15) Tang, W. C.; Lee, A. P. *Mater. Res. Soc. Bull.* **2001**, *26*, 318−319.
(16) de Boer, M. P.; Mayer, T. M. *Mater. Res. Soc. Bull.* **2001**, *26*, 302−304.
(17) Mastrangelo, C. H. *Tribol. Lett.* **1997**, *3*, 223−238.
(18) Kushmerick, J. G.; Hankins, M. G.; de Boer, M. P.; Clews, P. J.; Carpick, R. W.; Bunker, B. C. *Tribol. Lett.* **2001**, *10*, 103−108.
(19) Dugger, M. T.; Senft, D. C.; Nelson, G. C. Friction and Durability of Chemisorbed Organic Lubricants for MEMS. In *Microstructure and Tribology of Polymer Surfaces*; Tsukruk, V. V., Wahl, K. J., Eds.; American Chemical Society: Washington, DC, 1999.
(20) Houston, M. R.; Howe, R. T.; Komvopoulos, K.; Maboudian, R. *Mater. Res. Soc. Symp. Proc.* **1995**, *383*, 391−402.
(21) Carpick, R. W.; Salmeron, M. *Chem. Rev.* **1997**, *97*, 1163−1194 and references therein.
(22) Sullivan, J. P.; Friedmann, T. A.; Hjort, K. *Mater. Res. Soc. Bull.* **2001**, *26*, 309−311.
(23) Kohn, E.; Gluche, P.; Adamschik, M. *Diamond Relat. Mater.* **1999**, *8*, 934−940.
(24) Erdemir, A.; Eryilmaz, O. L.; Fenske, G. *J. Vac. Sci. Technol., A* **2000**, *18*, 1987−1992.
(25) Erdemir, A.; Fenski, G. R.; Krauss, A. R.; Gruen, D. M.; McCauley, T.; Csencsits, R. T. *Surf. Coat. Technol.* **1999**, *120*−*121*, 565−572.
(26) Gao, G. T.; Mikulski, P. T.; Harrison, J. A. *J. Am. Chem. Soc.* **2002**, *124*, 7202−7209.
(27) Brenner, D. W. *Phys. Rev. B* **1990**, *42*, 9458−9471.
(28) Brenner, D. W.; Harrison, J. A.; Colton, R. J.; White, C. T. *Thin Solid Films* **1991**, *206*, 220−223.
(29) Brenner, D. W. *Phys. Status Solidi B* **2000**, *217*, 23.
(30) Brenner, D. W.; Shenderova, O. A.; Harrison, J. A.; Stuart, S. J.; Ni, B.; Sinnott, S. B. *J. Phys. C* **2002**, *14*, 783−802.
(31) Berendsen, H. J. C.; Postma, J. P. M.; van Gunsteren, W. F.; DiNola, A.; Haak, J. *J. Chem. Phys.* **1984**, *81*, 3684−3690.
(32) Gear, C. W. *Numerical Initial Value Problems in Ordinary Differential Equations*; Prentice Hall: Englewood Cliffs, CA, 1971.
(33) Mikulski, P. T.; Harrison, J. A. *J. Am. Chem. Soc.* **2001**, *123*, 6873−6881.
(34) Kohary, K.; Kugler, S. *Phys. Rev. B* **2001**, *63*, 193404-1−193404-4.
(35) Kaukonen, H.-P.; Nieminen, R. M. *Phys. Rev. Lett.* **1992**, *68*, 620−623.
(36) Marks, N. A. *Phys. Rev. B* **2000**, *63*, 035401-1−035401-7.
(37) Sinnott, S. B.; Colton, R. J.; White, C. T.; Shenderova, O. A.; Brenner, D. W.; Harrison, J. A. *J. Vac. Sci. Technol., A* **1997**, *15*, 936−940.
(38) LiBassi, A.; Ferrari, A. C.; Stolojan, V.; Tanner, B. K.; Robertson, J.; Brown, L. M. *Diamond Relat. Mater.* **2000**, *9*, 771−776.
(39) Weiler, M.; Sattel, S.; Giessen, T.; Jung, K.; Ehrhardt, H. *Phys. Rev. B* **1996**, *53*, 1594−1608.
(40) Pharr, G. M.; Callahan, D. L.; McAdams, S. D.; Tsui, T. Y.; Anders, S.; Anders, A.; III, J. W. A.; Brown, I. G.; Bhatia, C. S.; Silva, S. R. P.; Robertson, J. *Appl. Phys. Lett.* **1996**, *68*, 779−781.
(41) Kelires, P. C. *Phys. Rev. Lett.* **1994**, *73*, 2460−2463.
(42) Ferrari, A. C.; Robertson, J.; Beghi, M. G.; Bottani, C. E.; Ferulano, R.; Pastorelli, R. *Appl. Phys. Lett.* **1999**, *75*, 1893−1895.
(43) Tomlinson, G. A. *Philos. Mag.* **1929**, *7*, 905.
(44) Frenkel, F. C.; Kontorova, T. *Zh. Eksp. Teor. Fiz.* **1938**, *8*, 1380.
(45) Harrison, J. A.; White, C. T.; Colton, R. J.; Brenner, D. W. *Phys. Rev. B* **1992**, *46*, 9700−9708.
(46) Scharf, T.; Singer, I. *Tribol. Lett.* **2003**, *14*, 137−145.
(47) Yen, B. K. *Wear* **1996**, *192*, 208.
(48) Donnett, C.; Grill, A. *Surf. Coat. Technol.* **1997**, *94*−*95*, 456−462.
(49) Erdemir, A. *Surf. Coat. Technol.* **2001**, *146*−*147*, 292−297.
(50) Grill, A.; Meyerson, B. S.; Patel, V. V.; Reimer, J. A.; Petrich, M. A. *J. Appl. Phys.* **1987**, *61*, 2874−2877.
(51) Kapitonov, I. N.; Konkov, O. I.; Terukov, E. I.; Trapeznikova, I. N. *Diamond Relat. Mater.* **2000**, *9*, 707−710.